Monatsh Chem (2012) 143:1687–1703
DOI 10.1007/s00706-012-0828-z

ORIGINAL PAPER

Remarkable influence of mild Lewis acid catalysts on cycloadditions leading to tetrasubstituted isoxazolidines: DFT analysis augmented by X-ray and NMR studies

Nivedita Acharjee · Avijit Banerji · Thierry Prangé

Received: 2 January 2012 / Accepted: 15 July 2012 / Published online: 8 September 2012

Abstract Experimental and theoretical studies were carried out to highlight the influence of mild Lewis acid catalysts on the cycloadditions leading to stereochemically defined tetrasubstituted isoxazolidines. Considerable acceleration and increased *exo* stereoselectivity were observed for lithium triflate and magnesium bromide catalyzed processes. DFT-based reactivity indices reflected the differences in polar character of the catalyzed and uncatalyzed pathways. The regioselectivities were predicted from interaction energy calculations. Finally, the transition states were successfully located and the extent of bond formation analyzed. The catalytic acceleration was rationalized by density functional theory (DFT) calculated activation parameters. The rate constant ratios with Eyring's transition state theory (TST) rate equation and total partition functions were also theoretically evaluated to further rationalize the observed catalytic acceleration.

Electronic supplementary material The online version of this article (doi:10.1007/s00706-012-0828-z) contains supplementary material, which is available to authorized users.

N. Acharjee
Department of Chemistry, Jalpaiguri Government Engineering College, Jalpaiguri 735102, West Bengal, India
e-mail: nivedita_acharjee@rediffmail.com

A. Banerji (✉)
Centre of Advanced Studies on Natural Products Including Organic Synthesis, Department of Chemistry, University of Calcutta, 92, Acharya Prafulla Chandra Road,
Kolkata 700009, India
e-mail: abnachem@rediffmail.com

T. Prangé
Laboratoire de Cristallographie et RMN biologiques (UMR 8015 CNRS), Université Paris Descartes,
4, av. de l'Observatoire, 75006 Paris, France

Keywords Catalysis · Density functional theory · Interaction energy · Transition states

Introduction

Catalytic studies of 1,3-dipolar cycloadditions (1,3DC) have gained wide significance in the last decade [1–5]. The need for regio- and stereospecific synthesis in natural product studies has encouraged the growth of this particular branch of 1,3DC chemistry. The reactions of C,N-disubstituted aldonitrones to α,β-unsaturated ketones generate tetrasubstituted isoxazolidines. These reactions are accelerated by coordination of the enone moiety to appropriate Lewis acid catalysts [6]. Consequently, the carbon–carbon double bond of the alkene becomes highly polarized with enhanced β-carbon electrophilicity. This induces a dramatic rate enhancement and sometimes leads to remarkable changes in the regio- and stereoselectivities. In the course of our study, it was interesting to note that the reaction rates and selectivities of the investigated cycloadditions changed remarkably in the presence of mild Lewis acid catalysts, e.g., metal triflates and magnesium bromide. Triflates were selected because they are most promising green chemistry catalysts, recoverable, and ensure better product separation. It was further possible to change the catalytic behavior as the well as the routine *endo* stereochemical pathway and hence promote *exo* selectivity by simple structural variations at the non-reacting site of the dipolarophile.

The aim of this work was to present a combined experimental and density functional theory (DFT)-based theoretical picture of some mild Lewis acid catalyzed 1,3DCs leading to tetrasubstituted isoxazolidines. The present report covers the experimental recordings (reaction conditions, total conversions, and product ratios) for the cycloaddition reactions, structure elucidation of the generated adducts (particularly by NMR and X-ray studies), analysis of the global and local (at the reactive sites) properties [7–17] of the reactants in the presence and absence of catalyst, interaction energy calculations from a perturbative orbital independent theoretical model [18], location of the stationary points for reactants, products, and transition states, and finally the determination of the activation parameters for the catalyzed and uncatalyzed processes in terms of DFT calculations. We then calculated the rate constant ratios from Eyring's transition state theory (TST) rate equation [19] and total partition functions [20] to underline the observed catalytic acceleration.

Results and discussion

Experimental results

The experimental data are collected in Table 1. The cycloaddition reaction of *C*-(4-chlorophenyl)-*N*-phenylnitrone (**1**) to anisalacetophenone (**5**) (Fig. 1) gave two diastereomeric products **8** and **9** in the ratio 92:8 with a total conversion of 74 % after 20 h as reported in our recent communication [21]. In the present study, when we carried out the reaction in the presence of lithium triflate, we observed a remarkable acceleration with a total conversion 91 % after 7 h. This can be attributed to the preferential complexation of anisalacetophenone to the lithium triflate catalyst. The diastereomeric excess of the *endo* adduct **8** over the *exo* isomer **9** was almost the same as in the case of the uncatalyzed reaction. In the presence of magnesium bromide, the conversion was 81 % after 3 h. However, a considerable decrease in the *endo* selectivity of the process occurred. The product ratio **8**:**9** was noted to be 58:42. Probably, the greater bulk of the magnesium bromide complexed unsaturated ketonic species inhibits the *endo* approach. It was rather surprising to note that the reaction was completely inhibited in the presence of ytterbium triflate and copper triflate to the limits of 300 MHz ^{1}H NMR detection.

The uncatalyzed cycloaddition reaction of *C*-(4-nitrophenyl)-*N*-phenylnitrone (**2**) to anisalacetophenone (**5**) afforded three cycloadducts **10**, **11**, and **12** in the ratio

Table 1 Experimental results for Lewis acid catalyzed cycloaddition reactions of C,N-disubstituted aldonitrones **1**–**4** to α,β-unsaturated ketones **5**–**7**

Run no.	Reactants	Additive	Time/h	Product ratios	Conversion/%
1	**1** + **5**	–	20	**8**:**9** = 92:8	74
2	**1** + **5**	Li(OTf)	7	**8**:**9** = 93:7	91
3	**1** + **5**	$MgBr_2 \cdot Et_2O$	3	**8**:**9** = 58:42	81
4	**1** + **5**	$Cu(OTf)_2$	28	Not detected	–
5	**1** + **5**	$Yb(OTf)_3$	28	Not detected	–
6	**2** + **5**	–	22	**10**:**11**:**12** = 85:10:5	79
7	**2** + **5**	Li(OTf)	8	**10**:**11**:**12** = 86:8:6	86
8	**2** + **5**	$Cu(OTf)_2$	28	Not detected	–
9	**2** + **5**	$Yb(OTf)_3$	28	Not detected	–
10	**2** + **6**	–	22	**13**:**14**:**15** = 81:10:9	79
11	**2** + **6**	Li(OTf)	7	**13**:**14**:**15** = 82:9:9	85
12	**2** + **6**	$Yb(OTf)_3$	28	Not detected	–
13	**2** + **6**	$Cu(OTf)_2$	28	Not detected	–
14	**3** + **6**	–	21	**16**:**17**:**18** = 77:14:9	80
15	**3** + **6**	Li(OTf)	7	**16**:**17**:**18** = 77:12:11	89
16	**3** + **6**	$Yb(OTf)_3$	28	Not detected	–
17	**3** + **6**	$Cu(OTf)_2$	28	Not detected	–
18	**1** + **7**	–	18	**19**:**20** = 87:13	81
19	**1** + **7**	Li(OTf)	7	**19**:**20** = 88:12	94
20	**1** + **7**	$Cu(OTf)_2$	3	**19**:**20** = 65:35	71
21	**1** + **7**	$Yb(OTf)_3$	3	**19**:**20** = 87:13	57
22	**4** + **6**	–	17	**21**:**22**:**23** = 78:8:14	65
23	**4** + **6**	Li(OTf)	7	**21**:**22**:**23** = 72:14:14	71
24	**4** + **6**	$MgBr_2 \cdot Et_2O$	7	**21**:**22**:**23** = 70:10:20	66
25	**4** + **6**	$Yb(OTf)_3$	28	Not detected	–
26	**4** + **6**	$Cu(OTf)_2$	28	Not detected	–

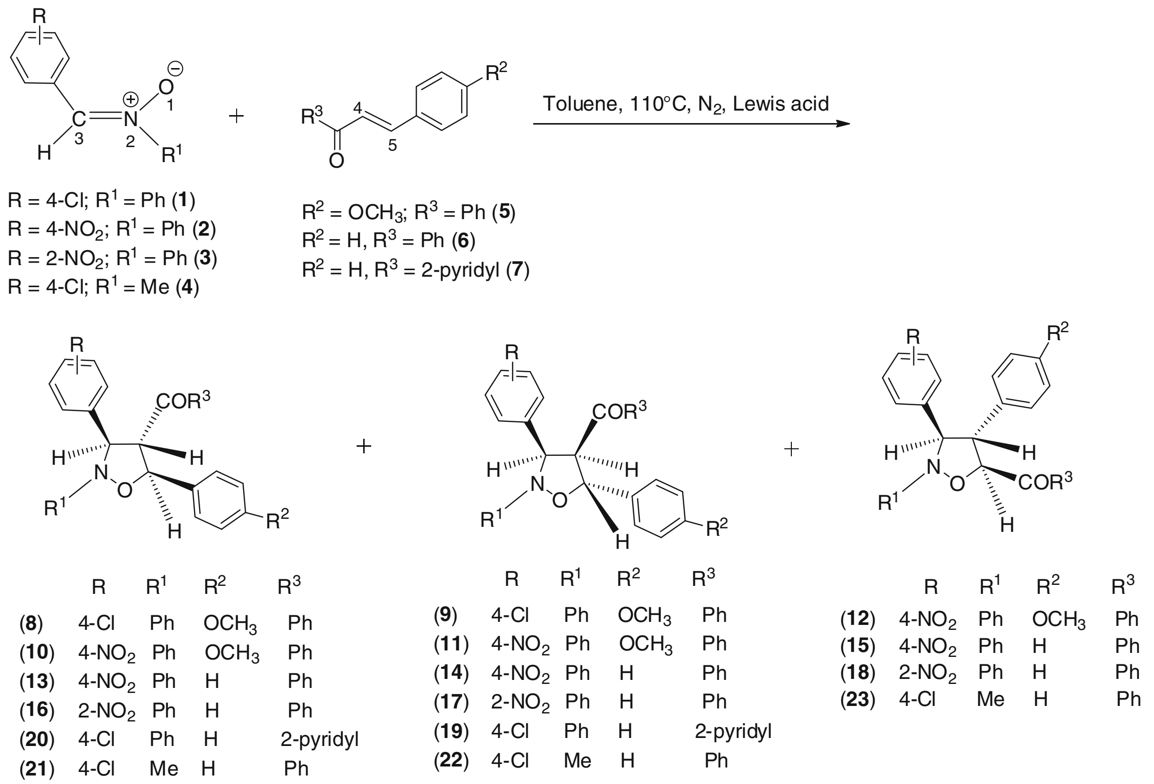

R = 4-Cl; R^1 = Ph (**1**)
R = 4-NO_2; R^1 = Ph (**2**)
R = 2-NO_2; R^1 = Ph (**3**)
R = 4-Cl; R^1 = Me (**4**)

R^2 = OCH_3; R^3 = Ph (**5**)
R^2 = H, R^3 = Ph (**6**)
R^2 = H, R^3 = 2-pyridyl (**7**)

	R	R^1	R^2	R^3
(**8**)	4-Cl	Ph	OCH_3	Ph
(**10**)	4-NO_2	Ph	OCH_3	Ph
(**13**)	4-NO_2	Ph	H	Ph
(**16**)	2-NO_2	Ph	H	Ph
(**20**)	4-Cl	Ph	H	2-pyridyl
(**21**)	4-Cl	Me	H	Ph

	R	R^1	R^2	R^3
(**9**)	4-Cl	Ph	OCH_3	Ph
(**11**)	4-NO_2	Ph	OCH_3	Ph
(**14**)	4-NO_2	Ph	H	Ph
(**17**)	2-NO_2	Ph	H	Ph
(**19**)	4-Cl	Ph	H	2-pyridyl
(**22**)	4-Cl	Me	H	Ph

	R	R^1	R^2	R^3
(**12**)	4-NO_2	Ph	OCH_3	Ph
(**15**)	4-NO_2	Ph	H	Ph
(**18**)	2-NO_2	Ph	H	Ph
(**23**)	4-Cl	Me	H	Ph

Fig. 1 Lewis acid catalyzed cycloaddition reactions of C,N-disubstituted aldonitrones **1**–**4** to α,β-unsaturated ketones **5**–**7**

85:10:5 with a total conversion 79 %. A 300 MHz ^{1}H NMR spectrum of the major *endo*/*meta* isomer **10** showed signals at $\delta = 5.51$ ppm (d, $J_{3,4} = 6.6$ Hz), 4.44 ppm (dd, $J_{3,4} = 6.6$ Hz, $J_{4,5} = 9.0$ Hz), and 5.21 ppm (d, $J_{4,5} = 9.0$ Hz) corresponding to H3, H4, and H5 of the isoxazolidine ring, respectively. The 3,4-*cis*-4,5-*trans* stereochemistry of cycloadduct **11** was determined by comparing the chemical shift values and coupling constants with those of similar cycloadducts isolated and analyzed in our previous studies [21, 22] and also those available in the literature [23] for reactions of benzylidene acetophenone. ^{1}H NMR signals for H3 and H5 of **12** were shielded by 0.18 and 0.61 ppm compared to those of cycloadduct **10** as expected from its regioisomeric structure in accordance with our previous studies [22]. The reaction between **2** and **5** gave 86 % yield after 7 h in the presence of lithium triflate and was completely inhibited in the presence of ytterbium triflate and copper triflate catalysts.

The reaction of nitrone **2** and benzylidene acetophenone (**6**) afforded three cycloadducts **13**, **14**, and **15** in the ratio 81:10:9 (total conversion 79 %). X-ray studies indicated the 3,4-*trans*-4,5-*trans* structure of **13** including the lone pair of nitrogen. The compound showed a pure O1 envelope (*E*) conformation. The ORTEP view and packing of **13** are shown in Fig. 2. We then carried out the reaction of *C*-(2-nitrophenyl)-*N*-phenylnitrone (**3**) and dipolarophile **6**. Three products **16**, **17**, and **18** were obtained in the ratio 77:14:9. The ORTEP view and packing of the molecule **16** are depicted in Fig. 2. X-ray diffraction studies indicated the all *trans* stereochemistry with a twist N2(O1) conformation. The minor 3,4-*cis* diastereomeric adduct **17** showed signals at $\delta = 5.89$ (d, $J_{3,4} = 9.3$ Hz), 5.02 (t, $J = 9.3$ Hz), and 5.80 ppm (d, $J_{4,5} = 9.3$ Hz) corresponding to H3, H4, and H5 of the isoxazolidine ring, respectively. The reaction systems **2**/**5**, **2**/**6**, and **3**/**6** were completely inhibited in the presence of ytterbium triflate and copper triflate and no product signals were detected in the 300 MHz ^{1}H NMR spectra of the crude reaction mixtures. The cycloaddition reactions of nitrones **1**–**6** were also carried out in acetonitrile. The uncatalyzed reactions did not occur in the presence of acetonitrile. We further observed only 1–3 % total conversion for the catalyzed reactions in acetonitrile and hence these were not pursued further.

The cycloaddition reaction of nitrone **1** to the benzylidene derivative of 2-acetylpyridine (**7**) was *exo* stereoselective, in contrast to the reactions of **5** and **6**, and afforded two diastereomeric cycloadducts **19** and **20** in the ratio 87:13 (total conversion 81 %) after 18 h. The 3,4-*cis*-4,5-*trans* stereochemistry of adduct **19** was determined from X-ray crystallographic analysis (Fig. 2). The compound showed an intermediate envelope/twist

Fig. 2 ORTEP view and packing of cycloadducts **13**, **16**, and **19**

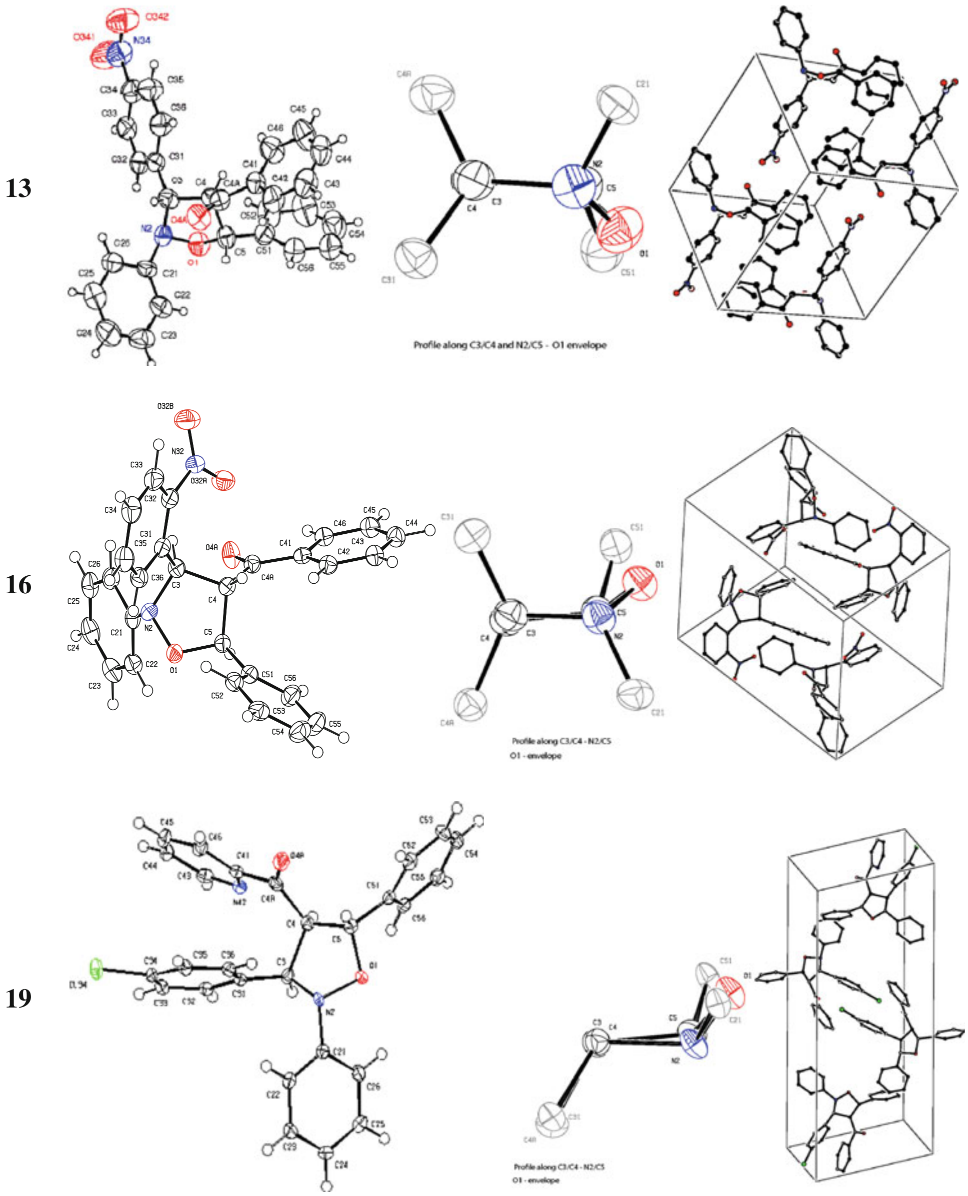

conformation with the O1 atom out of the mean plane defined by the four others.

H3, H4, and H5 of the minor *endo* adduct **20** appeared at $\delta = 5.40$, 5.20, and 6.00 ppm, respectively. Comparative chemical shift values of the isoxazolidine ring protons implied a diastereomeric relationship between **19** and **20**. In the presence of lithium triflate, the total conversion was 94 % after 7 h with 76 % de of the *exo* adduct **19** over the *endo* adduct **20**. When the reaction was carried out in the presence of ytterbium triflate, the total conversion was 57 % after 3 h with the product ratio **19**:**20** = 87:13. Copper triflate resulted in considerable reduction of the *exo* approach and the diastereomeric excess of *exo* adduct **19** over **20** was reduced to 30 % after 3 h. We then carried out the reaction between *C*-(4-chlorophenyl)-*N*-methylnitrone (**4**) and benzylideneacetophenone (**6**) in the presence of these catalysts. The uncatalyzed reaction (total conversion 65 %) afforded three adducts **21**, **22**, and **23** in the ratio 78:8:14 after 17 h [21]. The reaction time was reduced to 7 h in the presence of Li(OTf) and $MgBr_2{\cdot}Et_2O$ with a total conversion 71 and 66 %, respectively. No products were detected for ytterbium and copper triflate catalyzed reactions on the ^1H NMR spectra of crude reaction mixtures.

Irrespective of the *para* C-aryl substituents with varying electronic demand, the effective nitrone–Lewis acid complexation [6] probably blocked the cycloaddition pathway for nitrones **1** and **2** to α,β-unsaturated ketones **5** and **6**. However, dipolarophile **7** reacted with nitrone **1** in the presence of ytterbium and copper triflates. Presumably, this is due to preferential complexation of the Lewis acid catalysts to the latter.

Table 2 DFT/B3LYP/6-31G(d) calculated HOMO and LUMO energies and global properties of the reactants

	Optimized energy/au	HOMO/au	LUMO/au	μ/au	η/au	S/au	ω/eV
1	−1,091.512317	−0.207	−0.068	−0.139	0.257	1.946	1.023
5	−768.558418	−0.215	−0.065	−0.140	0.266	1.880	1.002
5-I	−1,737.641582	−0.230	−0.098	−0.166	0.244	2.049	1.536
5-II	−1,236.409799	−0.223	−0.095	−0.168	0.246	2.033	1.561
1-II	−1,559.359611	−0.218	−0.100	−0.169	0.251	1.992	1.548

Analysis based on electronic chemical potentials, global hardness, electrophilicity, and softness matching indices

Lithium triflate proved to be the best catalyst in terms of reaction time and total conversion of the investigated reactions. The lithium catalyzed reaction pathway is cost effective and appropriate to be investigated in terms of B3LYP/6-31G(d) level of theory unlike the other catalytic systems. Therefore, we have attempted to present a DFT interpretation for the uncatalyzed and lithium catalyzed reactions of nitrone **1** and dipolarophile **5**. The global properties are listed in Table 2. The $\mathrm{HOMO_{dipole}}$–$\mathrm{LUMO_{alkene}}$ and $\mathrm{HOMO_{alkene}}$–$\mathrm{LUMO_{dipole}}$ energy gaps for the **1/5** system are 372.8 and 385.9 kJ $\mathrm{mol^{-1}}$, respectively. The similarity of the $\mathrm{HOMO_{dipole}}$–$\mathrm{LUMO_{alkene}}$ and $\mathrm{HOMO_{alkene}}$–$\mathrm{LUMO_{dipole}}$ gaps for the reaction indicates that this reaction is of the intermediate type in Sustmann's classification (type II). Hence, the coordination of a Lewis acid to the dipole should also accelerate the reaction (at least from the molecular orbital theory viewpoint). We therefore attempted to consider both cases when lithium is coordinated to the dipole as well as to the dipolarophile molecule.

The electronic chemical potential μ is an index pointing to the direction of the electronic flux during the cycloaddition, i.e., the charge transfer (CT) within the system in the ground state. Definitions of electronic chemical potential (μ), hardness (η), softness (S), electrophilicity (ω), and Fukui functions (f_k^+, f_k^-) are available in many well-known reviews [24] and textbooks and need no further elaboration at this stage, except for their use and applications. The global indexes [7–12] are indicative of the polar character of a cycloaddition reaction especially in terms of the global electrophilicity difference $\Delta\omega$ between the reagents. Analysis of global electrophilicities can be used to choose the more appropriate computational model for Lewis acid catalyzed cycloadditions involving large molecules [25, 26].

5-I and **5**-II represent Li(OTf)- and LiCl-coordinated dipolarophile **5**, respectively. The electronic chemical potential μ of nitrone **1** ($\mu = -0.139$ au) is higher than **5**, **5**-I, and **5**-II, thereby unanimously indicating net charge transfer from dipole to dipolarophile. The low $\Delta\omega$ value (0.021 eV) for the **1/5** reaction system indicates a low polar character. Coordination of lithium metal to the oxygen atom of anisalacetophenone increases the electrophilicity of the corresponding complex. **5**-I has an electrophilicity value of 1.536 eV. **5**-II has an ω value of 1.561 eV. ω values of **5**-I and **5**-II allowed us to assert the use of the LiCl–anisalacetophenone complex **5**-II as a reduced model of **5**-I and hence required less computational effort in the transition state calculations. $\Delta\omega$ (0.5 eV) for the coordinated reaction systems **1/5**-I and **1/5**-II indicates a greater polar character compared to **1/5**. **1**-II represents LiCl-coordinated dipolarophile **1**. The $\mathrm{HOMO_{dipole}}$–$\mathrm{LUMO_{alkene}}$ energy gaps for **1/5**, **1/5**-II, and **1**-II**/5** systems are 372.8, 294.1, and 401.7 kJ $\mathrm{mol^{-1}}$ and $\mathrm{HOMO_{alkene}}$–$\mathrm{LUMO_{dipole}}$ gaps correspond to 385.9, 406.9, and 301.9 kJ $\mathrm{mol^{-1}}$, respectively. The coordination of alkene to Lewis acid decreases the $\mathrm{LUMO_{alkene}}$ energy and the $\mathrm{HOMO_{dipole}}$–$\mathrm{LUMO_{alkene}}$ gap. On the other hand, coordination of the dipole lowers the $\mathrm{HOMO_{alkene}}$–$\mathrm{LUMO_{dipole}}$ energy gap compared to the uncatalyzed reaction. Both possibilities suggest the acceleration of the reaction in the presence of the Lewis acid.

The condensed Fukui functions [15–17] (electrophilic and nucleophilic) of the reactants were calculated for the atomic sites in order to rationalize the observed regioselectivity in respect of the cycloadditions. Chandra and Nguyen [27] pointed out that the evaluation of condensed Fukui functions requires atomic electron population in a molecule, which is not an unambiguously defined quantity. They further reported that electrostatic potential driven atomic charges [28] and natural orbital-based charges [29] are more consistent for the calculation of Fukui functions. For the present study, we calculated the condensed Fukui functions on the basis of natural population analysis (NPA) [29] and Merz-Kollman (MK) [28] analysis. These are listed in Table 3. C_β has a larger ω_k than C_α in both the analyses. Therefore C_β will be the preferred position for the nucleophilic attack by the dipole. In the case of nitrone **1**, the f_k^- value from NPA and MK calculations of the oxygen atom O1 is greater than that of the carbon atom C3. This implies that nucleophilic attack of O1 of **1** at C_β of the dipolarophile is preferred in both **1/5** and **1/5**-II reaction systems. If we consider the **1**-II**/5** system, C3 of **1**-II has greater ω_k than O1 in both the analyses indicating nucleophilic attack by C_α (f_k^- value of C_α is greater than of C_β) of **5** at C3. Both these predictions lead to *meta* regioisomers in conformity with the experiments.

Table 3 DFT/B3LYP/6-31G(d) calculated local properties at the reactive site (k)

	k	f_k^+	s^+/au	ω_k^+/eV	f_k^-	s^-/au
NPA						
1	O1	0.099	0.193	0.101	0.217	0.422
	C3	0.123	0.239	0.126	0.125	0.243
MK						
1	O1	0.118	0.230	0.121	0.187	0.364
	C3	0.206	0.401	0.211	0.118	0.230
NPA						
5	C_α	0.028	0.053	0.028	0.126	0.237
	C_β	0.126	0.237	0.126	0.008	0.015
MK						
5	C_α	−0.006	−0.011	−0.006	0.156	0.293
	C_β	0.165	0.310	0.165	0.004	0.008
NPA						
1-II	O1	0.095	0.189	0.147	0.058	0.116
	C3	0.152	0.303	0.235	0.025	0.050
MK						
1-II	O1	0.175	0.345	0.271	0.028	0.056
	C3	0.292	0.581	0.452	0.034	0.068
NPA						
5-II	C_α	−0.017	−0.035	−0.027	0.051	0.104
	C_β	0.144	0.293	0.225	−0.020	−0.041
MK						
5-II	C_α	0.016	0.033	0.025	0.039	0.079
	C_β	0.168	0.342	0.262	0.017	0.035

Table 4 DFT/B3LYP/6-31G(d) calculated softness matching index for the catalyzed and uncatalyzed reactions

	1 + **5**	**1** + **5**-II	**1**-II + **5**
NPA			
Δ_{ortho}	0.136	0.211	0.085
Δ_{meta}	0.070	0.060	0.035
MK			
Δ_{ortho}	0.147	0.122	0.331
Δ_{meta}	0.061	0.039	0.197

Meta regioselectivity is also predicted from the lower value of softness matching index [14, 15, 21] Δ_{meta} compared to Δ_{ortho} for both the catalyzed and uncatalyzed reactions (Table 4).

Analysis based on the interaction energies between the reacting species

In the present study, we calculated the interaction energies between reactants to finally predict the regioselectivities by invoking a perturbative orbital independent theoretical model [18]. We recently applied the model to rationalize the regioselectivity of the cycloaddition reaction between *C*,*N*-diphenylnitrone and methyl crotonate [30]. In the present study, we considered two approaches to analyze the factor λ. The exact value of λ is difficult to determine with a simple model. The positive factor λ may be different for different 1,3-dipole–dipolarophile couples. Gazquez reported [31–33] that the value of λ was obtained by factors yielding at least an order of magnitude 1. Let this be coined as approach A. With approach A under consideration, the more important term is $\Delta E'_\mu$ as can be anticipated from the small difference in chemical potentials, especially for the uncatalyzed reaction.

Pal and Chandrakumar [34, 35] related the parameter λ to the change in the electron densities at the interacting site before and after the interaction process. This change will give the effective number of valence electrons that have participated in the interaction process. This can be termed as approach B. λ values calculated from Eq. 16 by NPA for the **1**/**5**, **1**/**5**-II, and **1**-II/**5** reaction systems are 0.021, 0.015, and 0.008, respectively. Approach B leads to comparable magnitudes of ΔE_υ and ΔE_μ for the catalyzed reaction channels. The calculated interaction energy values (Tables 5, 6) suggest that both the possibilities of electrophilic and nucleophilic attack at the dipole by the dipolarophile and vice versa need to be considered for the investigated reactions.

Let us analyze the preferred interactions between the electrophilic and nucleophilic sites of the reactants. The interaction energy $(\Delta E_{\text{int}})^k_{\text{dipole}}$ will be dominated by the local properties of the carbon and oxygen atoms of the dipoles. When we consider the local viewpoint for dipolarophiles, the interaction energy $(\Delta E_{\text{int}})^l_{\text{dipolarophile}}$ will be dominated by the local properties of C_α and C_β atoms. Both approach A and approach B predict interaction between C3 (electrophilic attack) of dipoles (**1**, **1**-II) and C_α (nucleophilic attack) of the dipolarophiles (**5**, **5**-II) by NPA and MK analyses. Considering the other way round, the interaction is prevalent between O1 (nucleophilic attack) of the dipoles and C_β (electrophilic attack) of the dipolarophiles. Both approach A and B imply the generation of *meta* regioisomers and hence are in agreement with the experiments.

Nature of transition states

Nitrone **1** preferably exists in *Z* configuration [36]. It is also well known that anisalacetophenone (**5**) exists exclusively in the *trans* form and hence was used as such in the computations. We attempted to locate the transition states (ts) for *endo* and *exo* approaches of **5** over (*Z*)-**1** in the present study along the regioisomeric reaction channels. tnm and txm indicate the *endo* and *exo* transition states for the uncatalyzed reaction along the *meta* pathway leading to products **8** (pn) and **9** (px), respectively (Fig. 3).

Table 5 Interaction energy values/kJ mol^{-1} for global–global interactions (ΔE_{int}), local–global interactions between dipoles and dipolarophiles ($(\Delta E_{\mathrm{int}})^k_{\mathrm{dipole}}$), and between dipolarophiles and dipoles ($(\Delta E_{\mathrm{int}})^l_{\mathrm{dipolarophile}}$)

ΔE	Global–global interactions	Local–global interactions between dipole **1** and dipolarophile **2**				Local–global interactions between dipolarophile **2** and dipole **1**			
		Nucleophilic attack at atom		Electrophilic attack at atom		Nucleophilic attack at atom		Electrophilic attack at atom	
		O1	C3	O1	C3	C_α	C_β	C_α	C_β
Reaction **1** + **5**									
NPA									
ΔE_υ	−0.001	−0.0002	−0.0003	−0.0005	−0.0003	−0.0001	−0.0003	−0.0003	−0.0000
$\Delta E'_\mu$	−343.113	−633.261	−619.514	−570.265	−618.347	−656.703	−601.351	−601.351	−669.429
Interaction energy	ΔE_{int}	$(\Delta E_{\mathrm{int}})^k_{\mathrm{dipole}}$				$(\Delta E_{\mathrm{int}})^l_{\mathrm{dipolarophile}}$			
	$-0.001-343.113\lambda$	$-0.0002-633.261\lambda$	$-0.0003-619.514\lambda$	$-0.0005-570.265\lambda$	$-0.0003-618.347\lambda$	$-0.0001-656.703\lambda$	$-0.0003-601.351\lambda$	$-0.0003-601.351\lambda$	$-0.0000-669.429\lambda$
MK									
ΔE_υ	−0.001	−0.0003	−0.0004	−0.0004	−0.0003	−0.0000	−0.0004	−0.0003	−0.0000
$\Delta E'_\mu$	−343.113	−622.156	−575.515	−585.004	−622.156	−678.424	−581.893	−586.311	−671.827
Interaction energy	ΔE_{int}	$(\Delta E_{\mathrm{int}})^k_{\mathrm{dipole}}$				$(\Delta E_{\mathrm{int}})^l_{\mathrm{dipolarophile}}$			
	$-0.001-343.113\lambda$	$-0.0003-622.156\lambda$	$-0.0004-575.515\lambda$	$-0.0004-585.004\lambda$	$-0.0003-622.156\lambda$	$-0.0000-678.424\lambda$	$-0.0004-581.893\lambda$	$-0.0003-586.311\lambda$	$-0.0000-671.827\lambda$
Reaction **1** + **5**-II									
NPA									
ΔE_υ	−1.098	−0.1943	−0.2365	−0.3861	−0.2399	−0.0389	−0.2809	−0.1087	−0.0459
$\Delta E'_\mu$	−329.920	−589.735	−577.795	−534.725	−576.779	−686.944	−586.311	−640.366	−689.108
Interaction energy	ΔE_{int}	$(\Delta E_{\mathrm{int}})^k_{\mathrm{dipole}}$				$(\Delta E_{\mathrm{int}})^l_{\mathrm{dipolarophile}}$			
	$-1.098-329.920\lambda$	$-0.1943-589.735\lambda$	$-0.2365-577.795\lambda$	$-0.3861-534.725\lambda$	$-0.2399-576.779\lambda$	$-0.0389-686.944\lambda$	$-0.2809-586.311\lambda$	$-0.1087-640.366\lambda$	$-0.0459-689.108\lambda$
MK									
ΔE_υ	−1.098	−0.0586	−0.2416	−0.2416	−0.0171	−0.0353	−0.3207	−0.0841	−0.0375
$\Delta E'_\mu$	−329.920	−629.013	−576.273	−576.273	−640.678	−663.340	−573.754	−648.272	−662.670
Interaction energy	ΔE_{int}	$(\Delta E_{\mathrm{int}})^k_{\mathrm{dipole}}$				$(\Delta E_{\mathrm{int}})^l_{\mathrm{dipolarophile}}$			
	$-1.098-329.920\lambda$	$-0.0586-629.013\lambda$	$-0.2416-576.273\lambda$	$-0.2416-576.273\lambda$	$-0.0171-640.678\lambda$	$-0.0353-663.340\lambda$	$-0.3207-573.754\lambda$	$-0.0841-648.272\lambda$	$-0.0375-662.670\lambda$
Reaction **1**-II + **5**									
NPA									
ΔE_υ	−1.0678	−0.1898	−0.2879	−0.1201	−0.0540	−0.0570	−0.2336	−0.2336	−0.0165
$\Delta E'_\mu$	−339.037	−634.485	−601.351	−657.690	−680.181	−641.932	−588.677	−588.677	−654.086
Interaction energy	ΔE_{int}	$(\Delta E_{\mathrm{int}})^k_{\mathrm{dipole}}$				$(\Delta E_{\mathrm{int}})^l_{\mathrm{dipolarophile}}$			
	$-1.0678-339.037\lambda$	$-0.1898-634.485\lambda$	$-0.2879-601.351\lambda$	$-0.1201-657.690\lambda$	$-0.0540-680.181\lambda$	$-0.0570-641.932\lambda$	$-0.2336-588.677\lambda$	$-0.1087-640.366\lambda$	$-0.0165-654.086\lambda$
MK									
ΔE_υ	−1.0678	−0.3245	−0.4904	−0.0598	−0.0722	0.0125	−0.2963	−0.2823	−0.0083
$\Delta E'_\mu$	−339.037	−588.677	−533.205	−678.073	−673.896	−662.670	−570.265	−574.508	−656.375
Interaction energy	ΔE_{int}	$(\Delta E_{\mathrm{int}})^k_{\mathrm{dipole}}$				$(\Delta E_{\mathrm{int}})^l_{\mathrm{dipolarophile}}$			
	$-1.0678-339.037\lambda$	$-0.3245-588.677\lambda$	$-0.4904-533.205\lambda$	$-0.0598-678.073\lambda$	$-0.0722-673.896\lambda$	$0.0125-662.670\lambda$	$-0.2963-570.265\lambda$	$-0.2823-574.508\lambda$	$-0.0083-656.375\lambda$

tno and txo indicate the corresponding transition states along the *ortho* pathway. For tnm and txm, the lengths of C–O forming bonds (2.132 and 2.118 Å) are shorter than those of C–C forming bonds (2.137 and 2.153 Å) (Table 7) (Fig. 4). The Wiberg and atom–atom overlap weighted natural atomic orbitals (NAO) bond order values indicate asynchronicity for the concerted cycloaddition processes. Jasiński et al. [37] also reported that B3LYP/6-

Table 6 Interaction energy values/kJ mol^{-1} for global–global interactions (ΔE_{int}; Eq. (14)), local–global interactions between dipoles and dipolarophiles ($(\Delta E_{\mathrm{int}})^{k}_{\mathrm{dipole}}$; Eq. (15)), and between dipolarophiles and dipoles ($(\Delta E_{\mathrm{int}})^{l}_{\mathrm{dipolarophile}}$; Eq. (15)) ($\lambda$ calculated from Eq. (16) in each case)

ΔE	Global–global interactions	Local–global interactions between dipole **1** and dipolarophile **2**				Local–global interactions between dipolarophile **2** and dipole **1**			
		Nucleophilic attack at atom		Electrophilic attack at atom		Nucleophilic attack at atom		Electrophilic attack at atom	
		O1	C3	O1	C3	C_{α}	C_{β}	C_{α}	C_{β}
Reaction **1** + **5**									
NPA									
ΔE_{υ}	−0.001	−0.0002	−0.0003	−0.0005	−0.0003	−0.0001	−0.0003	−0.0003	−0.0000
ΔE_{μ}	−3.603	−6.649	−6.505	−5.988	−6.493	−6.895	−6.314	−6.314	−7.029
Interaction energy	ΔE_{int}	$(\Delta E_{\mathrm{int}})^{k}_{\mathrm{dipole}}$				$(\Delta E_{\mathrm{int}})^{l}_{\mathrm{dipolarophile}}$			
	−3.604	−6.649	−6.505	−5.988	−6.493	−6.895	−6.314	−6.314	−7.029
MK									
ΔE_{υ}	−0.001	−0.0003	−0.0004	−0.0004	−0.0003	−0.0000	−0.0004	−0.0003	−0.0000
ΔE_{μ}	−3.603	−6.533	−6.043	−6.143	−6.533	−7.123	−6.110	−6.157	−7.054
Interaction energy	ΔE_{int}	$(\Delta E_{\mathrm{int}})^{k}_{\mathrm{dipole}}$				$(\Delta E_{\mathrm{int}})^{l}_{\mathrm{dipolarophile}}$			
	−3.603	−6.533	−6.043	−6.143	−6.533	−7.123	−6.110	−6.157	−7.054
Reaction **1** + **5**-II									
NPA									
ΔE_{υ}	−1.098	−0.1943	−0.2365	−0.3861	−0.2399	−0.0389	−0.2809	−0.1087	−0.0459
ΔE_{μ}	−2.474	−4.423	−4.333	−4.010	−4.326	−5.152	−4.397	−4.803	−5.168
Interaction energy	ΔE_{int}	$(\Delta E_{\mathrm{int}})^{k}_{\mathrm{dipole}}$				$(\Delta E_{\mathrm{int}})^{l}_{\mathrm{dipolarophile}}$			
	−3.572	−4.617	−4.570	−4.397	−4.566	−5.191	−4.678	−4.911	−5.214
MK									
ΔE_{υ}	−1.098	−0.0586	−0.2416	−0.2416	−0.0171	−0.0353	−0.3207	−0.0841	−0.0375
ΔE_{μ}	−2.474	−4.718	−4.322	−4.322	−4.805	−4.975	−4.303	−4.862	−4.970
Interaction energy	ΔE_{int}	$(\Delta E_{\mathrm{int}})^{k}_{\mathrm{dipole}}$				$(\Delta E_{\mathrm{int}})^{l}_{\mathrm{dipolarophile}}$			
	−3.572	−4.776	−4.564	−4.564	−4.822	−5.010	−4.624	−4.946	−5.010
Reaction **1**-II + **5**									
NPA									
ΔE_{υ}	−1.0678	−0.1898	−0.2879	−0.1201	−0.0540	−0.0570	−0.2336	−0.2336	−0.0165
ΔE_{μ}	−1.356	−2.538	−2.405	−2.630	−2.721	−2.568	−2.355	−2.355	−2.616
Interaction energy	ΔE_{int}	$(\Delta E_{\mathrm{int}})^{k}_{\mathrm{dipole}}$				$(\Delta E_{\mathrm{int}})^{l}_{\mathrm{dipolarophile}}$			
	−2.424	−2.728	−2.693	−2.751	−2.774	−2.624	−2.588	−2.588	−2.633
MK									
ΔE_{υ}	−1.0678	−0.3245	−0.4904	−0.0598	−0.0722	0.0125	−0.2963	−0.2823	−0.0083
ΔE_{μ}	−1.356	−2.355	−2.133	−2.712	−2.695	−2.651	−2.281	−2.298	−2.626
Interaction energy	ΔE_{int}	$(\Delta E_{\mathrm{int}})^{k}_{\mathrm{dipole}}$				$(\Delta E_{\mathrm{int}})^{l}_{\mathrm{dipolarophile}}$			
	−2.424	−2.679	−2.623	−2.772	−2.768	−2.638	−2.577	−2.580	−2.626

31G(d) calculations perfectly illustrate the structure of transition states in cycloadditions between diarylnitrones and 1-EWG-2-arylethenes.

Jasiński et al. [38] reported the application of bond development indices $I_{\mathrm{C3-C4}}$ and $I_{\mathrm{C5-O1}}$ calculated by the relations

$$I_{\mathrm{C3-C4}} = 1 - [\{r^{\mathrm{TS}}_{\mathrm{C3-C4}} - r^{\mathrm{P}}_{\mathrm{C3-C4}}\}/r^{\mathrm{P}}_{\mathrm{C3-C4}}]$$

$$I_{\mathrm{C5-O1}} = 1 - [\{r^{\mathrm{TS}}_{\mathrm{C5-O1}} - r^{\mathrm{P}}_{\mathrm{C5-O1}}\}/r^{\mathrm{P}}_{\mathrm{C5-O1}}]$$

to explain the bond formation in cycloaddition reactions of 2-nitro-1-propene to (*Z*)-*C*,*N*-diarylnitrones. They further defined asymmetry indices Δa as the absolute values of the differences between $I_{\mathrm{C3-C4}}$ and $I_{\mathrm{C5-O1}}$. In the present study, the calculated $I_{\mathrm{C3-C4}}$ and $I_{\mathrm{C5-O1}}$ (Table 7) indicate that for tnm, txm, tno, and txo, the C3–C4 bond forms more rapidly than the C5–O1 bond. The asymmetry indices Δa follow the order tno > tnm > txm > txo for the cycloaddition reaction. The index t was estimated by the relation given by

Fig. 3 *Endo*/*meta* approach for reaction systems **1**/**5**, **1**/**5**-II, and **1**-II/**5**

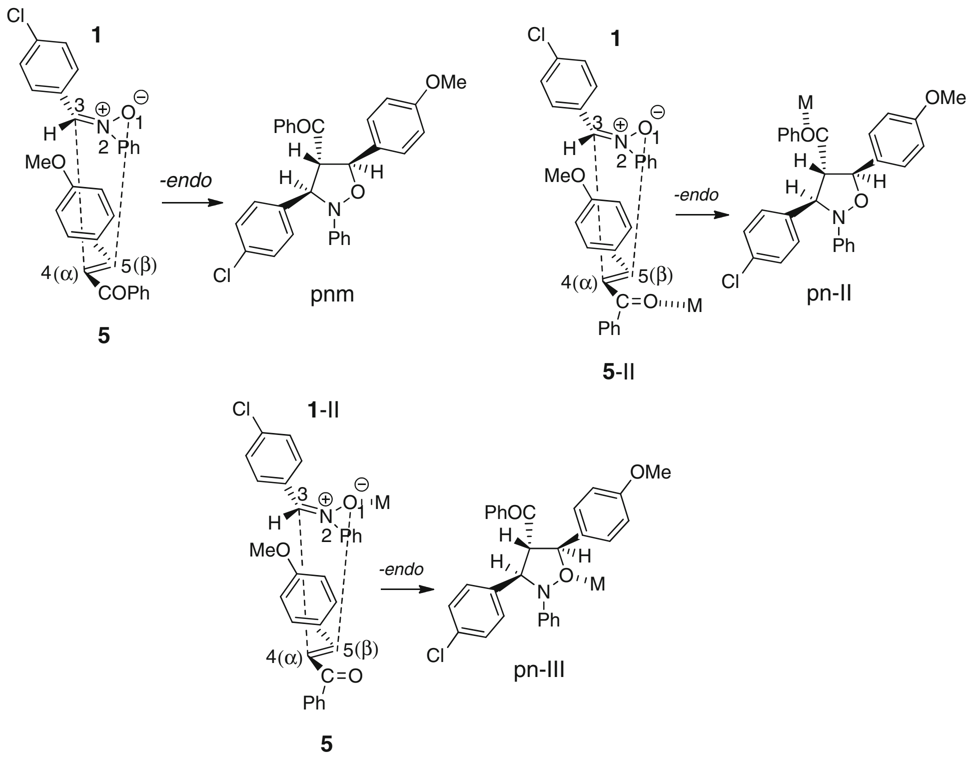

Table 7 Bond lengths (r/Å), Wiberg bond indices (a), atom–atom overlap weighted NAO bond orders (b), charge transfer (CT), bond development indices (I), and asymmetry indices (Δa) of the located transition states

ts	O1–N1	N2–C3	C3–C4	C4–C5	C5–O1	$a_{C3–C4}$	$a_{C5–O1}$	$b_{C3–C4}$	$b_{C5–O1}$	$I_{C3–C4}$	$I_{C5–O1}$	Δa	CT
tnm	1.311	1.363	2.137	1.415	2.132	0.406	0.333	0.332	0.202	0.640	0.535	0.105	0.029
txm	1.313	1.364	2.153	1.417	2.118	0.409	0.342	0.328	0.214	0.635	0.546	0.089	0.022
tno	1.301	1.372	2.093	1.413	2.126	0.446	0.327	0.366	0.201	0.666	0.522	0.144	0.024
txo	1.306	1.367	2.197	1.413	2.070	0.396	0.362	0.314	0.228	0.597	0.553	0.044	0.001
tnII	1.351	1.345	2.384	1.451	1.717	0.278	0.597	0.211	0.440	0.494	0.818	0.324	0.148
tnIII	1.325	1.371	2.034	1.417	2.252	0.484	0.258	0.403	0.150	0.708	0.473	0.235	−0.153

Leroy et al. [39]; $t = -\Sigma q_A$ where q_A is the net charge and the sum is taken over all the atoms of the dipolarophile. The charge transferred t for both *endo* (0.029 e, 0.024 e) and *exo* (0.022 e, 0.001 e) reaction channels reveal an almost neutral reaction and an electron flow from the nitrone to the dipolarophile. This is in agreement with the electronic chemical potential values (Table 2). We then focused our attention on the lithium catalyzed process. The *endo*/*meta* pathway (leading to the major adduct) has been studied with dipolarophile–Lewis acid (P1) and dipole–Lewis acid (P2) coordination possibilities. tn-II and tn-III represent transition states for P1 and P2 reaction channels. The electron flow indicated by t values for tn-II (0.148 e) and tn-III (−0.153 e) agree well with the electronic chemical potentials and electrophilicities (Table 2). The transition state tn-II showed considerable asynchronicity compared to tn as is evident from the bond orders of the forming C–O and C–C bonds. The forming C–O bond in tn-II has a shorter bond length (1.717 Å) value than that of the forming C–C bond (2.384 Å). However, the forming C3–C4 bond is shorter than C5–O1 for the tn-III transition state. Bond development indices indicate more rapid C5–O1 bond formation than C3–C4 for tn-II. On the other hand, $I_{C3–C4}$ is calculated to be greater than $I_{C5–O1}$ for tn-III. It is interesting to note here that asynchronicity of the forming C–O and C–C bonds experiences a crossover for the uncoordinated to dipolarophile-coordinated transition state but not for the dipole-coordinated channel. The catalyzed transition states tn-II and tn-III have greater asymmetry indices Δa compared to tnm.

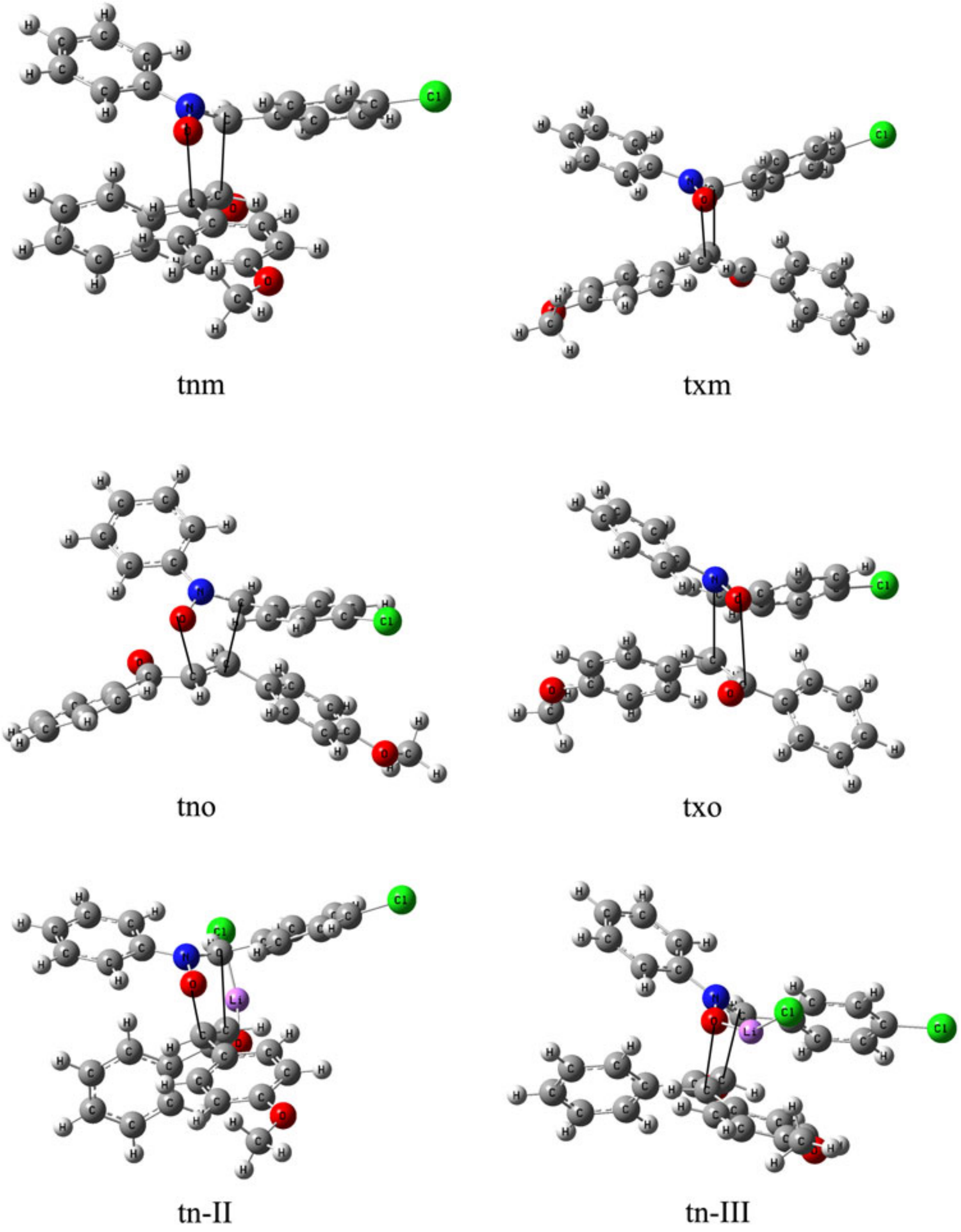
tnm txm

tno txo

tn-II tn-III

Fig. 4 DFT/B3LYP/6-31G(d) calculated transition states for the cycloaddition reactions

Analysis based on activation parameters and rate constants

The activation energy of transition state tnm is 6.6 kJ mol^{-1} lower than that of txm (Table 8). The free energy of activation $\Delta G^{\#}$ for the predicted *endo*/*meta* channel along the uncatalyzed process is lower than the corresponding *exo* attack by 8.3 kJ mol^{-1} (Table 9). These calculations agree well with the experimentally determined 84 % de of the *endo* adduct **8** (pnm) over the *exo* isomer **9** (pxm). Figure 5a presents ΔE and ΔG reaction profiles for these two reaction channels.

The *endo* product pnm is thermodynamically more stable than pxm by 13.7 kJ mol^{-1}. Large entropies of activation are a necessary condition for multicentered concerted cycloaddition reactions [40]. This is evident for the calculated entropies of activations (−195 to −202 J mol^{-1} K^{-1}) for all four reaction channels. Analysis of the relative energies presented in Table 8 indicates that B3LYP calculations do not clearly predict the regioselectivity of this 1,3DC. This inability to predict the regioselectivity of 1,3DCs reliably has also come up in the study of other related reactions [41]. Domingo et al. [42] reported similar results for nitrone cycloaddition reactions to acrylonitrile. Domingo et al. [43] further concluded that regioselectivity predictions are highly dependent on the computational levels but all computational levels predict correct stereoselectivities for the preferred channel.

Table 8 B3LYP/6-31G(d) calculated energies for the reaction channels

Configuration of the approaching reactants	Optimized product energies/au	Transition states			
		ts	Optimized energies/au	Activation energy/kJ mol^{-1}	
				Gas phase	Toluene
1 + **5** (*endo*/*meta*)	−1,860.084916	tnm	−1,860.036118	90.887	101.629
1 + **5** (*exo*/*meta*)	−1,860.079711	txm	−1,860.033620	97.445	106.334
1 + **5** (*endo*/*ortho*)	−1,860.086701	tno	−1,860.039146	82.937	93.788
1 + **5** (*exo*/*ortho*)	−1,860.088029	txo	−1,860.029347	108.664	118.247
1 + **5**-II (*endo*/*meta*)	−2,327.924386	tn-II	−2,327.893474	75.200	96.101
1-II + **5** (*endo*/*meta*)	−2,327.923059	tn-III	−2,327.884103	89.074	121.823

Table 9 DFT/B3LYP/6-31G(d) calculated free energy and enthalpy changes along the different paths

Reacting channel	$\Delta G^{\#}$/ kJ mol^{-1}	$\Delta H^{\#}$/ kJ mol^{-1}	$\Delta S^{\#}$/J mol^{-1} K^{-1}
Endo/*meta* [**5**/**1**]	151.657	93.119	−196.432
Exo/*meta* [**5**/**1**]	159.903	99.690	−202.058
Endo/*ortho* [**5**/**1**]	143.746	84.704	−198.123
Exo/*ortho* [**5**/**1**]	168.559	110.232	−195.461
Endo/*meta* [**5**-II/**1**]	139.199	76.982	−217.622
Endo/*meta* [**1**-II/**5**]	155.934	91.081	−208.781

The observed *endo* selectivity is probably the outcome of the steric interactions between the aryl group in the C3 position and the electron-withdrawing benzoyl group in the C4 position and the stabilizing secondary orbital interactions between p_z orbitals on the aryl rings in the 3 and 5 positions. This has been pointed out for the reactions of (*Z*)-*C*,*N*-diphenylnitrone and (*E*)-2-arylnitroethenes [43]. Gandolfi et al. [44, 45] critically analyzed the importance of secondary orbital interactions in favoring the *endo* mode for dipolar cycloadditions.

We also noted the generation of pre-reaction complexes at the initial stage on all of the investigated pathways. The relative energies of these complexes are shown in Fig. 5.

The presence of coordinated dipolarophile **5** decreases $\Delta G^{\#}$ by 12.5 kJ mol^{-1} along the *endo*/*meta* channel (Table 9). However, the dipole coordination increases the free energy of activation by 4.3 kJ mol^{-1}. The small differences between $\Delta E^{\#}$ and $\Delta H^{\#}$ of tnm and tn-III do not allow the quantitative evaluation of the results. However, $\Delta E^{\#}$ and $\Delta H^{\#}$ of tn-II are lower those that of tnm by 15.7 and 16.1 kJ mol^{-1}, respectively. This is clearly evident from the reaction profile Fig. 5b. In the present study, the rate constant ratios k_1/k_2, k_3/k_1, k_4/k_1 (Table 10) were calculated from both partition functions (Eq. 18) and free energy of activations (Eq. 19) and are listed in Table 10. The results were found to be in good agreement with each other. These values suggest faster reactions for dipolarophile coordination and retardation in the case of dipole coordination for the favored *endo*/*meta* channel.

Domingo et al. [42, 46–48] reported solvent effect considerations by B3LYP/6-31G(d) single point calculations on the gas-phase structures using a self-consistent reaction field (SCRF) [49] based on the polarizable continuum model (PCM) of Tomasi's group [50–52] to calculate ΔE values for cycloaddition reactions of diphenylnitrone to acrolein [46] and maleimide [46], carbonyl ylides to 1,2-benzoquinone [48], cyclic nitrone to methyl propiolate and acrylonitrile [42], etc. We have also reported similar calculations for the reactions of nitrone **1** to benzylideneacetophenone [21]. We similarly calculated ΔE for the present reaction channels in toluene with the dielectric constant 2.379 at 298.15 K. These are collected in Table 8. tnm has a lower activation energy than txm by 4.7 kJ mol^{-1} in toluene. The dipole coordination increases the activation barrier of the *endo*/*meta* channel by 20.2 kJ mol^{-1} in toluene. On the contrary, the energy of activation is lowered by 5.5 kJ mol^{-1} by dipolarophile coordination. It is also evident that B3LYP calculations do not clearly predict regioselectivities for this 1,3DC even after inclusion of solvent effects. However, regiochemistries predicted by local electrophilicities, softness matching indices, and interaction energy calculations are found to be in conformity with the experimental findings.

Although from the molecular orbital point of view the cycloaddition reaction appears to be Sustmann type II and hence should be accelerated by both dipole and dipolarophile coordinations, it is only the latter coordination which accelerates the reaction by lowering the activation parameters and dipole coordination retards the cycloaddition process. Probably, the limited rate increase at high temperature (110 °C) is an outcome of the competitive coordination of the dipole and dipolarophile with the employed Lewis acid catalyst and hence does not seem to be compatible with the typical catalytic effects.

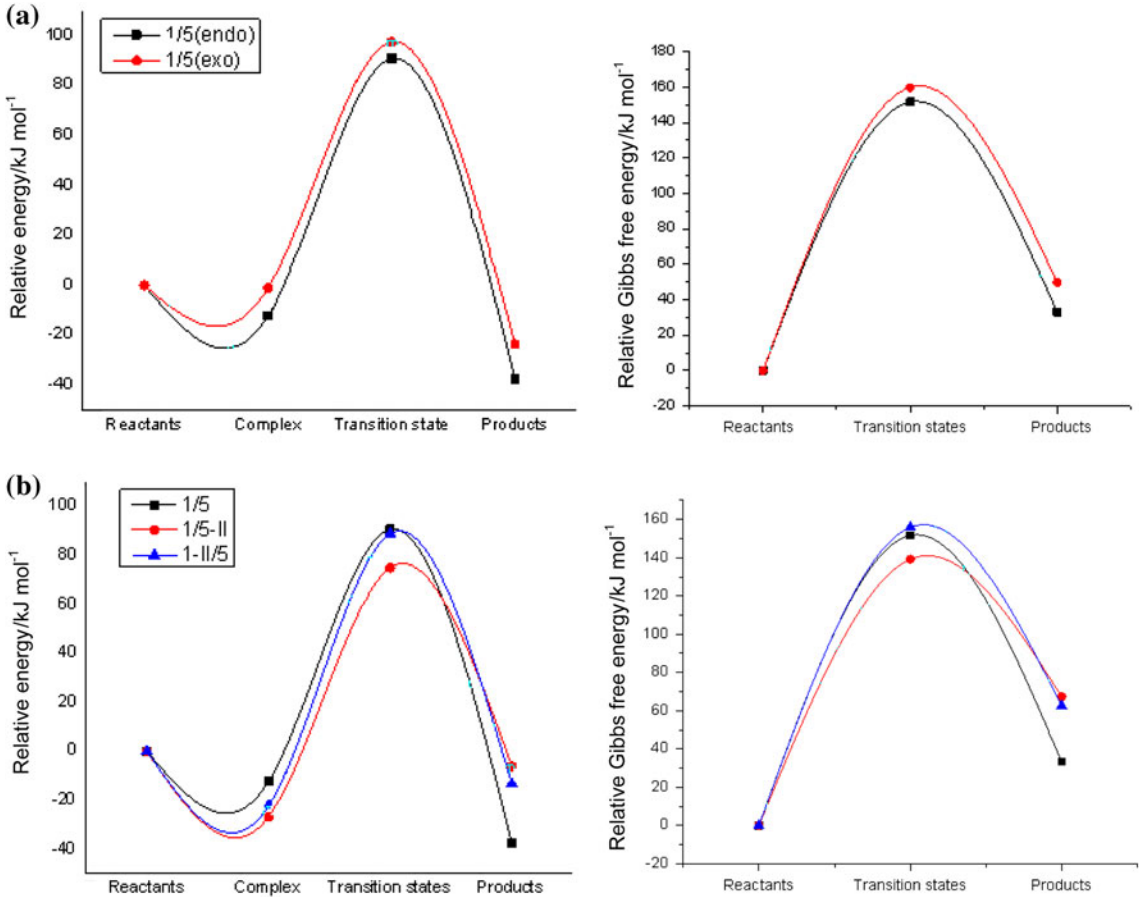

Fig. 5 Reaction profiles for the investigated reaction paths: **a** ΔG and ΔE for the uncatalyzed reaction channels; **b** ΔG and ΔE for the uncatalyzed (I), dipole-coordinated (II), and dipolarophile-coordinated (III) reaction channels along the *endo*/*meta* pathway

Table 10 Rate constant ratios for the reaction paths

Ratios	Calculated from Eq. (18)	Calculated from Eq. (19)
Endo/*meta* [**5**/**1**] (k_1):*exo*/*meta* [**5**/**1**] (k_2)	2.7874×10^{1}	2.6992×10^{1}
Endo/*meta* [**1**-II/**5**] (k_3):*endo*/*meta* [**5**/**1**] (k_1)	1.7459×10^{-1}	1.7782×10^{-1}
Endo/*meta* [**5**-II/**1**] (k_4):*endo*/*meta* [**5**/**1**] (k_1)	1.5200×10^{2}	1.5707×10^{2}

Experimental

UV spectra were recorded in dry acetonitrile using a Shimadzu UV-3101 PC spectrophotometer. IR spectra were recorded in KBr pellets using a Perkin Elmer RX-9 FT-IR spectrophotometer. Melting points were recorded on an electrically heated Kofler Block apparatus. 300 MHz ^{1}H NMR and 75.5 MHz ^{13}C NMR spectra were recorded on a Bruker AV-300 NMR spectrometer. 500 MHz ^{1}H NMR, 125.5 MHz ^{13}C NMR, DQF-COSY, HMQC, and HMBC spectra were recorded on a Bruker DRX500 NMR spectrometer. Mass spectra are recorded with a JEOL JMS600 mass spectrometer.

Procedure for the cycloaddition reactions

Each of the dipoles (0.0044 mol; 1.02 g **1**, 1.06 g **2**, 1.06 g **3**, and 0.75 g **4** [53]) was allowed to react with 0.0066 mol of the dipolarophiles (1.57 g **5** [54, 55], 1.37 g **6**, and 1.38 g **7**) in 5 cm^{3} refluxing dry thiophene-free toluene under a nitrogen atmosphere. Dipolarophiles **5** and **6** were obtained from mixed aldol condensation of benzaldehyde/anisaldehyde and acetophenone [54, 55]. Compound **7** was prepared from aldol condensation of benzaldehyde and 2-acetylpyridine at 5 °C. Each cycloaddition reaction used 0.00088 mol of the catalysts (0.14 g lithium triflate, 0.16 g magnesium bromide, 0.55 g ytterbium triflate, and 0.32 g copper triflate). Magnesium bromide was dissolved in a minimum quantity of diethyl ether and then added to the solution. Each reaction was monitored at regular time intervals by analyzing aliquots by TLC and 300 MHz ^{1}H NMR spectroscopy. After the run time was over, toluene was removed under reduced pressure and the crude reaction mixtures were subjected to column chromatography over neutral alumina to separate the cycloadducts. ^{1}H NMR signals for compounds **12**, **14**, **15**, and **17** were detected in the 300 MHz ^{1}H NMR spectra of the crude reaction mixtures prior to column chromatography. The column was initially eluted in each case with petroleum ether (b.p. 60–80 °C) and then with petroleum ether/benzene mixtures progressively increasing the proportion of benzene in the eluent. We recently reported [21] the isolation, properties, and spectroscopic data for cycloadducts **8**, **9**, **21**, **22**, and **23** and hence have not repeated them here.

(3α,4β,5α)-4-Benzoyl-5-(4-methoxyphenyl)-3-(4-nitrophenyl)-2-phenylisoxazolidine (**10**, $C_{29}H_{24}N_2O_5$)

Bright yellow crystals; yield 1.22 g (58 %); isolated from 30 % benzene in petroleum ether/benzene = 4:1 eluates; m.p.: 146 °C; IR (KBr): $\bar{\nu}$ = 3,077 (w), 1,670 (s), 1,520 (s), 1,347 (s), 1,251 (s), 827 (m), 752 (s), 692 (s) cm^{-1}; ^{1}H NMR (300 MHz, $CDCl_3$): δ = 3.77 (s, OCH_3), 5.51 (d, J = 6.6 Hz, H3), 4.44 (dd, J = 6.6, 9.0 Hz, H4), 5.21 (d, J = 9.0 Hz, H5), 6.97 (d, J = 7.8 Hz, H2,6(A)), 6.93 (t, J = 7.4 Hz, H4(A)), 7.62 (d, J = 8.8 Hz, H2,6(B)), 8.18 (d, J = 8.8 Hz, H3,5(B)), 7.36 (d, J = 7.0 Hz, H2,6(C)), 7.11–7.27 (m, H3,5(A), H3,4,5(C), H2,6(D)), 6.76 (d, J = 7.8 Hz, H3,5(D)) ppm; ^{13}C NMR (75.5 MHz, $CDCl_3$): δ = 55.30 (OCH_3), 73.83 (C3), 69.27 (C4), 85.06 (C5), 151.01 (C1(A)), 114.18, 114.07 (C2,6(A), C3,5(D)), 127.26 (C3,5(A)), 122.18 (C4(A)), 149.26 (C1(B)), 124.31 (C3,5(B)), 147.51 (C4(B)), 136.00 (C1(C)), 133.92 (C4(C)), 130.19 (C1(D)), 160.24 (C4(D)), 128.32, 128.56, 128.69, 129.19 (C2,6(B), C2,6(C), C3,5(C), C2,6(D)), 195.80 (C=O) ppm; MS: m/z = 480 [$C_{29}H_{24}N_2O_5$, M^+], 239 [$C_{16}H_{14}O_2H^+$], 131 [$C_9H_7O^+$], 105 [$C_7H_5O^+$], 91 [$C_7H_7^+$], 77 [$C_6H_5^+$], 51 [$C_4H_3^+$].

(3α,4β,5α)-4-Benzoyl-5-(4-methoxyphenyl)-3-(4-nitrophenyl)-2-phenylisoxazolidine (**11**, $C_{29}H_{24}N_2O_5$)

Yellow amorphous powder; yield 0.13 g (6 %); isolated from 30 % benzene in petroleum ether/benzene = 4:1 eluates after removing the crystals of **10**; IR (KBr): $\bar{\nu}$ = 3,078 (w), 1,672 (s), 1,525 (s), 1,349 (s), 1,254 (s), 828 (m), 748 (s), 690 (s) cm^{-1}; ^{1}H NMR (300 MHz, $CDCl_3$): δ = 3.80 (s, OCH_3), 5.83 (d, J = 10.2 Hz, H3), 4.60 (dd, J = 10.2, 9.6 Hz, H4), 5.15 (d, J = 9.6 Hz, H5), 6.94 (d, J = 7.9 Hz, H2,6(A)), 6.96 (m, H4(A)), 7.60 (d, J = 8.9 Hz, H2,6(B)), 8.16 (d, J = 8.9 Hz, H3,5(B)), 7.46 (d, J = 7.0 Hz, H2,6(C)), 7.09–7.24 (m, H3,5(A), H3,4,5(C), H2,6(D)), 6.72 (d, J = 7.9 Hz, H3,5(D)) ppm; ^{13}C NMR (75.5 MHz, $CDCl_3$): δ = 54.99 (OCH_3), 70.34 (C3), 65.85 (C4), 81.94 (C5), 148.73 (C1(A)), 115.82 (C2,6(A)), 127.51 (C3,5(A)), 122.85 (C4(A)), 146.82 (C1(B)), 123.47 (C3,5(B)), 147.50 (C4(B)), 135.85 (C1(C)), 134.14 (C4(C)), 129.87 (C1(D)), 114.07 (C3,5(D)), 160.45 (C4(D)), 128.69, 129.15, 129.38, 129.46 (C2,6(B), C2,6(C), C3,5(C), C2,6(D)), 195.80 (C=O) ppm; MS: m/z = 480 [$C_{29}H_{24}N_2O_5$, M^+], 239 [$C_{16}H_{14}O_2H^+$], 131 [$C_9H_7O^+$], 105 [$C_7H_5O^+$], 91 [$C_7H_7^+$].

(3α,4β,5α)-4-Benzoyl-3-(4-nitrophenyl)-2,5-diphenylisoxazolidine (**13**, $C_{28}H_{22}N_2O_4$)

Pale yellow crystals; yield 1.13 g (57 %); isolated from 20 % benzene in petroleum ether/benzene = 4:1 eluates; m.p.: 132 °C; UV–Vis (acetonitrile, $c = 5 \times 10^{-5}$ mol dm^{-3}): λ_{max} (log ε) = 249 (4.02) nm; IR (KBr): $\bar{\nu}$ = 3,057 (w), 1,679 (s), 1,519 (s), 1,343 (s), 827 (m), 755 (s), 694 (s) cm^{-1}; ^{1}H NMR (300 MHz, $CDCl_3$): δ = 5.61 (d, J = 6.8 Hz, H3), 4.58 (dd, J = 6.8, 9.0 Hz, H4), 5.38 (d, J = 9.0 Hz, H5), 7.07 (d, J = 7.9 Hz, H2,6(A)), 7.21–7.31 (dist. t, m, H3,5(A)), 7.05 (dist. d, H4(A)), 7.73 (d, J = 8.6 Hz, H2,6(B)), 8.25 (d, J = 8.6 Hz, H3, 5(B)), 7.46 (dist. d, H2,6(C)), 7.29–7.40 (m, H3,4,5(C), H2,3,4,5,6(D)) ppm; ^{13}C NMR (75.5 MHz, $CDCl_3$): δ = 73.87 (C3), 69.39 (C4), 85.09 (C5), 150.92 (C1(A)), 114.18 (C2,6(A)), 127.32 (C3,5(A)), 122.31 (C4(A)), 149.07 (C1(B)), 124.32 (C3,5(B)), 147.54 (C4(B)), 135.76, 135.98 (C1(C), C1(D)), 133.96 (C4(C)), 126.81 (C2,6(D)), 129.13 (C4(D)), 128.56, 128.67, 128.87, 129.20 (C2,6(B), C2,6(C), C3,5(C), C3,5(D)), 195.80 (C=O) ppm; MS: m/z = 450 [$C_{28}H_{22}N_2O_4$, M^+], 242 [$C_{13}H_{10}N_2O_3$], 209 [$C_{15}H_{12}OH^+$], 131 [$C_9H_7O^+$], 105 [$C_7H_5O^+$], 93 [$C_6H_5O^+$], 77 [$C_6H_5^+$], 51 [$C_4H_3^+$].

(3α,4β,5α)-4-Benzoyl-3-(2-nitrophenyl)-2,5-diphenylisoxazolidine (**16**, $C_{28}H_{22}N_2O_4$)

Pale yellow crystals; yield 1.11 g (56 %); isolated from 20 % benzene in petroleum ether/benzene = 4:1 eluates; m.p.: 174 °C; UV–Vis (acetonitrile, $c = 5 \times 10^{-5}$ mol dm^{-3}): λ_{max} (log ε) = 243 (3.98) nm; IR (KBr): $\bar{\nu}$ = 3,062 (w), 1,677 (s), 1,523 (s), 1,343 (s), 859 (w), 749 (s), 691 (s) cm^{-1}; ^{1}H NMR (500 MHz, $CDCl_3$): δ = 6.12 (d, J = 4.3 Hz, H3), 4.56 (dd, J = 4.3, 8.5 Hz, H4), 5.27 (d, J = 8.5 Hz, H5), 7.12 (dd, J = 7.7, 1.0 Hz, H2,6(A)), 7.34 (br. t, H3,5(A)), 7.01 (tt, J = 7.7, 1.0 Hz, H4(A)), 8.01 (dd, J = 8.0, 1.3 Hz, H3 (B)), 7.51 (td, J = 8.0, 1.3 Hz, H4(B)), 7.79 (td, J = 8.0, 1.3 Hz, H5(B)), 8.41 (dd, J = 8.0, 1.3 Hz, H6(B)), 7.44 (dist. d, H2,6(C)), 7.19 (t, J = 7.5 Hz, H3,5(C)), 7.41 (dist. t, J = 7.5 Hz, H4(C)), 7.24–7.34 (m, H2,3,4,5,6(D)) ppm; ^{13}C NMR (125.5 MHz, $CDCl_3$): δ = 71.71 (C3), 69.99 (C4), 86.44 (C5), 150.47 (C1(A)), 114.28 (C2,6(A)), 129.68 (C3,5(A)), 122.42 (C4(A)), 138.93 (C1(B)), 147.69 (C2(B)), 125.27 (C3(B)), 129.05 (C4(B)), 134.76 (C5(B)), 130.25 (C6(B)), 136.50, 136.48 (C1(C), C1(D)), 129.32 (C2,6(C)), 129.12 (C3,5(C)), 133.85 (C4(C)), 127.71 (C2,6(D)), 128.84 (C3,5(D)), 129.57 (C4(D)), 196.98 (C=O) ppm; MS: m/z = 450 [$C_{28}H_{22}N_2O_4$, M^+], 242 [$C_{13}H_{10}N_2O_3$], 209 [$C_{15}H_{12}OH^+$], 131

$[C_9H_7O^+]$, 105 $[C_7H_5O^+]$, 93 $[C_6H_5O^+]$, 77 $[C_6H_5{}^+]$, 51 $[C_4H_3{}^+]$.

(3α,4β,5α)-5-Benzoyl-3-(2-nitrophenyl)-2,4-diphenylisoxazolidine (**18**, $C_{28}H_{22}N_2O_4$)

Yellow amorphous powder; yield 0.08 g (4 %); isolated from 30 % benzene in petroleum ether/benzene = 4:1 eluates; IR (KBr): $\bar{\nu}$ = 3,060 (w), 1,676 (s), 1,522 (s), 1,340 (s), 860 (w), 751 (s), 690 (s) cm^{-1}; ^1H NMR (500 MHz, $CDCl_3$): δ = 5.70 (d, J = 5.9 Hz, H3), 4.33 (t, J = 5.9 Hz, H4), 5.45 (d, J = 5.9 Hz, H5), 7.06 (d, J = 7.7 Hz, H2,6(A)), 7.23 (br. t, H3,5(A)), 6.98 (t, J = 7.7 Hz, H4(A)), 7.99 (dd, J = 8.0, 1.2 Hz, H3(B)), 7.43 (td, J = 8.0, 1.2 Hz, H4(B)), 7.72 (td, J = 8.0, 1.2 Hz, H5(B)), 8.34 (dd, J = 8.0, 1.2 Hz, H6(B)), 7.39 (dist. d, H2,6(C)), 7.11 (t, J = 7.5 Hz, H3,5(C)), 7.35 (dist. t, J = 7.5 Hz, H4(C)), 7.14–7.32 (m, H2,3,4,5,6(D)) ppm; ^{13}C NMR (125.5 MHz, $CDCl_3$): δ = 74.11 (C3), 68.05 (C4), 85.42(C5), 151.21 (C1(A)), 114.74 (C2,6(A)), 121.78 (C4(A)), 137.89 (C1(B)), 148.11 (C2(B)), 125.42 (C3(B)), 129.11 (C4(B)), 134.81 (C5(B)), 130.76 (C6(B)), 135.95, 135.98 (C1(C)), C1(D)), 128.61, 129.86, 129.34, 128.79 (C3,5(A), C2,6(C), C3,5(C), (C3,5(D)), 133.91 (C4(C)), 127.84 (C2,6(D)), 129.32 (C4(D)), 197.00 (C=O) ppm; MS: m/z = 450 $[C_{28}H_{22}N_2O_4$, $M^+]$, 209 $[C_{15}H_{12}OH^+]$, 131 $[C_9H_7O^+]$, 105 $[C_7H_5O^+]$, 93 $[C_6H_5O^+]$, 77 $[C_6H_5{}^+]$.

(3α,4β,5α)-3-(4-Chlorophenyl)-4-(2-pyridinylcarbonyl)-2,5-diphenylisoxazolidine (**19**, $C_{27}H_{21}ClN_2O_2$)

White crystals; yield 1.20 g (62 %); isolated from 10 % benzene in petroleum ether eluates; m.p.: 66 °C; UV–Vis (acetonitrile, $c = 5 \times 10^{-5}$ mol dm^{-3}): λ_{max} (log ε) = 245 (4.00) nm; IR (KBr): $\bar{\nu}$ = 3,051 (w), 1,684 (s), 1,569 (s), 1,484 (s), 1,348 (s), 1,245 (s), 834 (m), 760 (s), 690 (s) cm^{-1}; ^1H NMR (300 MHz, $CDCl_3$): δ = 5.33 (d, J = 5.9 Hz, H3), 5.27 (dd, J = 5.9, 7.6 Hz, H4), 5.56 (d, J = 7.6 Hz, H5), 7.05 (dt, J = 7.8, 1.0 Hz, H2,6(A)), 7.24–7.28 (m, H3,5(A)), 6.97 (tt, J = 7.3, 1.0 Hz, H4(A)), 7.27–7.32 (m, H3,5(B)), 7.50 (d, J = 8.4 Hz, H2,6(B)), 7.97 (dt, J = 7.7, 1.0 Hz, H3(C)), 7.76 (td, J = 7.7, 1.7 Hz, H4(C)), 7.37 (ddd, J = 7.7, 4.7, 1.2 Hz, H5(C)), 8.36 (ddd, J = 4.7, 1.7, 0.9 Hz, H6(C)), 7.43 (dist. d, J = 7.7 Hz, H2,6(D)), 7.24–7.31 (m, H3,4,5(D)) ppm; ^{13}C NMR (125.5 MHz, $CDCl_3$): δ = 73.47 (C3), 67.04 (C4), 83.94 (C5), 151.48 (C1(A)), 114.88 (C2,6(A)), 122.36 (C4(A)), 140.73 (C1(B)), 133.62 (C4(B)), 152.66 (C2(C)), 123.16 (C3(C)), 137.33 (C4(C)), 127.86 (C5(C)), 149.14 (C6(C)), 137.33 (C1(D)), 127.51 (C2,6(D)), 128.80 (C4 (D)), 128.79, 128.83, 129.23, 129.41 (C3,5(A), C2,6(B), C3,5(B), C3,5(D)), 198.22 (C=O) ppm; MS: m/z = 440 $[C_{27}H_{21}ClN_2O_2$, $M^+]$, 231 $[C_{13}H_{10}ClNO]$, 210 $[C_{14}H_{11}NOH^+]$, 139, 131 $[C_9H_7O^+]$, 111 $[C_6H_4Cl^+]$, 105 $[C_7H_5O^+]$, 91 $[C_7H_7{}^+]$, 77 $[C_6H_5{}^+]$, 51 $[C_4H_3{}^+]$.

X-ray structure determination

Compound **13** was isolated as bundles of imbricate crystals. One of the small masses was dispersed in oil (Nujol) and crunched. It appeared that small pieces of debris were pure monocrystals under polarized light. One of these small plates with approximate size 10 μm was captured with a nylon loop whilst observing under a microscope. As it was anticipated that a standard diffractometer would not be sensitive enough, measurements were done at the ESRF synchrotron source in Grenoble. The crystal was mounted at the end of the BM 14 beam line operating a QUANTUM ADSC detector, tuned to a wavelength of 0.9615 Å. Diffraction data were processed using the HKL suite of programs. The structure was refined with the SHELXL [56] program, using isotropic then anisotropic thermal parameters. The hydrogen atoms were localised on Fourier difference maps and introduced with an isotropic thermal factor equal to that of the bonded atom. Compounds **16** and **19** were dispersed in paraffin oil and selected crystals were mounted in cryo-loops and stored at 100 K in liquid nitrogen. Recording parameters on beam line ID 29 were adjusted to adapt with the atomic resolution diffracting crystals. The structures were refined using the same protocol: isotropic atoms first, then location of hydrogens on difference-Fourier maps, then refinements with anisotropic thermal factors for non-hydrogen atoms.

13: System: triclinic (space group $P1$, $Z = 2$); cell parameters: a = 9.390(1) Å, b = 11.540(1) Å, c = 11.701 (1) Å, α = 100.74(4)°, β = 100.66(4)°, γ = 108.53(4)°, V = 1139.7(2) $Å^3$.

16: System: monoclinic (space group $P21/n$, $Z = 4$); cell parameters: a = 10.304(1) Å, b = 17.286(2) Å, c = 13.027(1) Å, α = 90°, β = 97.74(5)°; γ = 90°, V = 2299.2(3) $Å^3$.

19 System: monoclinic (space group $P21/c$, $Z = 4$); cell parameters: a = 5.980(1) Å, b = 11.750(1) Å, c = 30.301 (2) Å, α = 95.14(4)°, V = 2120.5(4) $Å^3$.

X-ray data of **13**, **16**, and **19** have been deposited at the Cambridge Structural Data Centre under CCDC numbers 765672, 787238, and 787239, respectively. The data can be obtained free of charge via http://www.ccdc.cam.ac.uk/data_request/cif or by e-mailing data_request@ccdc.cam.ac.uk, or by contacting The Cambridge Crystallographic Data Centre, 12, Union Road, Cambridge CB2 1EZ, UK; fax: +44-1223-336033.

Computational methods

The electronic chemical potential μ [7] and chemical hardness η [8] can be evaluated from the ionization potential (I) [57] and electron affinity (A) [57] as

$$\mu \approx -(I + A)/2 \tag{1}$$

$$\eta \approx I - A \tag{2}$$

The global electrophilicity index ω [9–12] can be simply expressed by

$$\omega = \mu^2/2\eta \tag{3}$$

The global softness S is given by [11]

$$S = 1/2\eta \tag{4}$$

Fukui functions [13, 14] (for nucleophilic [f_k^+] and electrophilic [f_k^-] attack) of an atom in a molecule can be written in terms of the respective electron populations of the cationic, neutral, and anionic systems.

For nucleophilic attack

$$f_k^+ = q_k(N + 1) - q_k(N) \tag{5}$$

For electrophilic attack

$$f_k^- = q_k(N) - q_k(N - 1) \tag{6}$$

The local electrophilicity index ω_k [12–15] is given by $\omega_k = \omega f_k^+$. The local softnesses [s^+, s^-] are calculated as the product of global softness S and the respective Fukui functions.

$$s_k^+ = Sf_k^+; s_k^- = Sf_k \tag{7}$$

The softness matching index Δ_{ij}^{kl} is given by

$$\Delta_{ij}^{kl} = (s_i^- - s_k^+)^2 + (s_j^- - s_l^+)^2 \tag{8}$$

where atoms i and j of the nucleophile interact with atoms k and l of the electrophile, respectively, to give rise to the preferred regioisomer. The reaction pathway involving lower value of Δ_{ij}^{kl} will be the favored one.

When a stable molecule A (formed by bonding of K atoms, N_A being the total number of electrons in A) and a stable molecule B (formed by bonding of L atoms, N_B being the total number of electrons in B) interact with each other, the interaction energy [18] from DFT is given by

$$\Delta E_{\text{int}} = \Delta E_\upsilon + \Delta E_\mu$$

where ΔE_υ and ΔE_μ are the energy changes at constant external potential and constant chemical potential, respectively, and are written as

$$\Delta E_\upsilon \approx -1/2[\{ S_A S_B[\mu_A - \mu_B]^2\}/\{ S_A + S_B\}] \tag{9}$$

$$\Delta E_\mu \approx -1/2[\lambda/\{S_A + S_B\}] \tag{10}$$

where μ, η, and S are derived from Eqs. (1), (2), and (6), respectively. When we invoke the local viewpoint of one reactant, ΔE_υ, and ΔE_μ in terms of condensed Fukui function f_k become

$$\Delta E_\upsilon \approx -1/2 [\{ S_A S_B f_k[\mu_A - \mu_B]^2\}/\{S_A f_k + S_B\}] \tag{11}$$

$$\Delta E_\mu \approx -1/2[\lambda/\{f_k S_A + S_B\}] \tag{12}$$

The interaction energy $(\Delta E_{\text{int}})_A^k$ can be rewritten in shorthand notation as

$$(\Delta E_{\text{int}})_A^k \approx \Delta E_\upsilon + \lambda \Delta E'_\mu \text{ with } \Delta E'_\mu = \Delta E_\mu(\lambda = 1). \tag{13}$$

The parameter λ has been related to the deviation of total softness of the interacting system AB from the sum of the softnesses of individual systems A and B. It has been defined somewhat arbitrarily in the literature [31–33]. In the present study, following the work of Mendez et al. [18] we initially assumed here that λ is close to 1 and ΔE_μ is much more important than ΔE_υ.

Pal and Chandrakumar [34, 35] related the parameter λ to the change in the electron densities at the interacting site before and after the interaction process and calculated the global and local interaction energies as given by Eqs. (16) and (17).

$$\Delta E_{\text{int}} \approx \frac{-(\mu_A - \mu_B)^2}{2}\left(\frac{S_A S_B}{S_A + S_B}\right)_v - \frac{1}{4}\left(\frac{\lambda}{S_A + S_B}\right)_\mu \tag{14}$$

$$(\Delta E_{\text{int}})_{Ax} \approx \frac{-(\mu_A - \mu_B)^2}{2}\left(\frac{S_A f_{Ax} S_B}{S_A f_{Ax} + S_B}\right)_v - \frac{1}{4}\left(\frac{\lambda}{S_A f_{Ax} + S_B}\right)_\mu \tag{15}$$

This change will give the effective number of valence electrons that have participated in the interaction process. Gazquez also pointed out that the factor λ is proportional to an effective number of valence electrons [31–33] taking part in the reaction. An expression for the term λ can be written as the difference of electron densities of the system A before and after the interaction [34, 35]:

$$\lambda_A = \sum_{i=1}^{p} \rho_{Ai}^{\text{eq}} - \sum_{i=1}^{p} \rho_{Ai}^{0} \tag{16}$$

Alternately, the term λ can be defined as the difference of electron densities for system B

$$\lambda_B = \sum_{j=1}^{q} \rho_{Bj}^{\text{eq}} - \sum_{j=1}^{q} \rho_{Bj}^{0} \tag{17}$$

where the first terms of the right-hand side of the Eqs. (16) and (17) refer to the sum of the electron densities of each atom in A and B in the molecule AB at equilibrium, respectively, and the second terms in Eqs. (16) and (17) refer to electron densities of each atom in the isolated systems A and B, respectively. The indices p and q are the number of atoms of the systems A and B, respectively. With this approach, λ appears to be much less than 1 and ΔE_μ and ΔE_υ may be quite comparable.

The geometries were optimized by DFT with Becke's [58] three-parameter hybrid exchange functional in combination with the gradient-corrected correlation functional of Lee et al. [59] (B3LYP) using the 6-31G(d) basis set. The transition states were localized at DFT/B3LYP/6-31G(d) level of theory. The stationary points were characterized through vibrational frequency analysis done at 298.15 K at the DFT/B3LYP/6-31G(d) level. All the stationary points are definitely identified for minima (number of imaginary frequencies = 0) or transition states (number of imaginary frequencies = 1). In accordance with our previous studies [60], intrinsic reaction coordinate (IRC) [61, 62] calculations were performed to verify that the energy curve connecting the optimized reactants and the products passes through the correct and the lowest TS which must be a first-order saddle point. The electron affinity and ionization potential were obtained at similar level using UB3LYP theory for the anion and cation. The geometries of the neutral species are used to calculate the electronic structure of the charged species in order to fulfill the demand for constant external potential. The electronic populations were computed from NPA [29] and also by the charges derived from the electrostatic potential according to MK algorithm [28].

Apart from activation barrier calculations, it would be very desirable to theoretically evaluate the rate constant ratios for elementary bimolecular reactions in the gas phase. According to the theory of reaction rates [20], the rate constant for reaction $[\mathrm{A} + \mathrm{B} \rightleftharpoons \mathrm{AB}^{\#} \rightarrow \text{products}]$ between A and B is given by

$$k = \frac{k_{\mathrm{B}}T}{h}\frac{Q^{\#}}{Q_{\mathrm{A}}Q_{\mathrm{B}}}e^{-E_{\mathrm{a}}/\mathrm{RT}} \tag{18}$$

where Q values represent the total partition constants and E_{a} the activation energy. Rate constants can also be calculated with the simple Eyring equation [18], derived from transition state theory:

$$k = \frac{k_{\mathrm{B}}T}{h}e^{-\Delta G^{\#}/RT} \tag{19}$$

where $\Delta G^{\#}$ represents the free energy of activation at 298 K.

All calculations were carried out using the Gaussian 2003 [63] set of programs along with the graphical interface Gauss View 2003.

Acknowledgments Nivedita Acharjee is grateful to the University Grants Commission, India (project no F.PSW-111/11-12 (ERO)) for financial support to carry out the experimental and theoretical catalytic investigations. The kind cooperation of Prof. Manas Banerjee of Burdwan University, West Bengal, India is greatly acknowledged.

References

1. Gothelf AS, Gothelf KV, Hazell RG, Jørgensen KA (2002) Angew Chem Int Ed 41:4236
2. Huang ZZ, Kang YB, Zhou J, Ye MC, Tang T (2004) Org Lett 6:1677
3. Suga H, Nakajima T, Itoh K, Kakehi A (2005) Org Lett 7:1431
4. Chow SS, Nevalainen M, Evans CA, Johannes CW (2007) Tetrahedron Lett 48:277
5. Padwa A, Pearson WH (2002) Synthetic applications of 1,3-dipolar cycloaddition chemistry towards heterocycles and natural products. Wiley, New York
6. Gothelf KV (2002) In: Kobayashi S, Jorgensen KA (eds) Cycloaddition reactions in organic chemistry. Wiley, Weinheim, p 211
7. Parr RG, Yang W (1989) In: Density functional theory of atoms and molecules. Oxford University Press, New York
8. Parr RG, Pearson RG (1983) J Am Chem Soc 105:7512
9. Parr RG, Szentpaly LV, Liu S (1999) J Am Chem Soc 121:1922
10. Pérez P, Domingo LR, Aurell MJ, Contreras R (2003) Tetrahedron 59:3117
11. Benchouk W, Mekelleche SM (2008) J Mol Struct (Theochem) 852:46
12. Chattaraj PK, Sarkar U, Roy DR (2006) Chem Rev 106:2065
13. Yang W, Mortier WJ (1986) J Am Chem Soc 108:5708
14. Chandra AK, Nguyen MT (1997) J Chem Soc, Perkin Trans 2:1415
15. Zhang YL, Yang ZZ (2000) J Mol Struct (Theochem) 496:139
16. Aurell MJ, Domingo LR, Pérez P, Contreras R (2004) Tetrahedron 60:11503
17. Merino P, Revuelta J, Tejero T, Chiacchio U, Rescifina U, Romeo G (2003) Tetrahedron 60:3581
18. Méndez F, Tamariz J, Geerlings P (1998) J Phys Chem A 102:6292
19. McQuarrie DA, Simon JD (1998) Physical chemistry, 1st South Asian edn. Viva Books, New Delhi
20. Laidler KJ (2009) Chemical kinetics, 3rd edn. Pearson Education, Singapore
21. Acharjee N, Banerji A, Prangé T (2010) Monatsh Chem 141:1213
22. Banerji A, Maiti KK, Haldar S, Mukhopadhyay C, Banerji J, Prangé T, Neumann A (2000) Monatsh Chem 131:901
23. Sridharan V, Muthusubramanium S, Sivasubramanian S, Polborn K (2004) Tetrahedron 60:8881
24. Kohn W, Sham L (1965) Phys Rev 140A:1133
25. Domingo LR, Chamorro E, Pérez P (2008) J Org Chem 73:4615
26. Domingo LR, Asensio A, Arroyo P (2002) J Phys Org Chem 15:660
27. Chandra AK, Nguyen MT (2002) Int J Mol Sci 3:310
28. Besler BH, Merz KM Jr, Kollman PA (1990) J Comput Chem 11:431
29. Reed AE, Weinhold F (1983) J Chem Phys 78:4066
30. Acharjee N, Banerji A (2011) Comput Theor Chem 967:50
31. Parr RG, Gázquez JL (1993) J Phys Chem 97:3939
32. Gazquez JL, Martinez A, Mendez F (1993) J Phys Chem 97:4059
33. Gazquez JL (2003) In: Sen KD (ed) Chemical hardness: structure and bonding, vol 80. Springer, New York, p 27
34. Pal S, Chandrakumar KRS (2000) J Am Chem Soc 122:4145
35. Pal S, Chandrakumar KRS (2002) J Phys Chem A 106:5737
36. Koyano K, Suzuki H (1969) Bull Soc Chem Jpn 42:3306
37. Barański A, Lyubimtsev A, Jasiński R, Kwiatkowska M (2008) Polish J Chem 82:1037
38. Jasiński R, Wąsika K, Mikulskaa M, Barański A (2009) J Phys Org Chem 22:717
39. Leroy G, Sana M, Burke LA, Nguyen MT (1980) Quantum Theory Chem React 1:91
40. Husigen R (1976) J Org Chem 41:403
41. Cossio P, Morao I, Jiao H, Schleyer PVR (1999) J Am Chem Soc 121:6737
42. Carda M, Portolés R, Murga J, Uriel S, Marco JA, Domingo LR, Zaragoźa RJ, Röper H (2000) J Org Chem 65:7000
43. Baranski A, Jasinski R (2001) Chem Heterocycl Comp 37:1518

44. Burdisso M, Gandolfi R, Grünanger P (1990) J Org Chem 55:3429
45. Baldwin JE, Reddy PV (1989) J Org Chem 54:5264
46. Domingo LR, Benchouk W, Mekelleche SM (2007) Tetrahedron 63:4464
47. Domingo LR, Aurell MJ, Arnó M, Sáez JA (2007) J Mol Struct (Theochem) 811:125
48. Domingo LR, Aurell MJ, Pérez P, Sáez JA (2012) RSC Adv 2:1334
49. Tomasi J, Persico M (1994) Chem Rev 94:2027
50. Cances E, Mennucci B, Tomasi J (1997) J Chem Phys 107:3032
51. Cossi M, Barone V, Cammi R, Tomasi J (1996) Chem Phys Lett 255:327
52. Barone V, Cossi M, Tomasi J (1998) Comput Chem 19:404
53. Banerji A, Biswas PK, Sengupta P, Dasgupta S, Gupta M (2004) Indian J Chem 43B:880
54. Kohler EP, Chadwell HM (1922) Org Synth 2:1
55. Kohler EP, Chadwell HM (1941) Org Synth Coll 1:78
56. Sheldrick GM, Schneider TR (1997) Methods Enzymol 277:319
57. Domingo LR, Sáez JA, Pérez P (2007) Chem Phys Lett 438:341
58. Becke AD (1993) J Chem Phys 98:5648
59. Lee C, Yang W, Parr RG (1988) Phys Rev B 37:785
60. Acharjee N, Das TK, Banerji A, Banerjee M, Prangé T (2010) J Phys Org Chem 23:1187
61. Gonzalez C, Schlegel HB (1989) J Phys Chem 90:2154
62. Gonzalez C, Schlegel HB (1990) J Phys Chem 94:5523
63. Frisch MJ, Trucks GW, Schlegel HB, Scuseria GE, Robb MA, Cheeseman JR, Montgomery JA Jr, Vreven T, Kudin KN, Burant JC, Millam JM, Iyengar SS, Tomasi J, Barone V, Mennucci B, Cossi M, Scalmani G, Rega N, Petersson GA, Nakatsuji H, Hada M, Ehara M, Toyota K, Fukuda R, Hasegawa J, Ishida M, Nakajima T, Honda Y, Kitao O, Nakai H, Klene M, Li X, Knox JE, Hratchian HP, Cross JB, Adamo C, Jaramillo J, Gomperts R, Stratmann RE, Yazyev O, Austin AJ, Cammi R, Pomelli C, Ochterski JW, Ayala PY, Morokuma K, Voth GA, Salvador P, Dannenberg JJ, Zakrzewski VG, Dapprich S, Daniels AD, Strain MC, Farkas O, Malick DK, Rabuck AD, Raghavachari K, Foresman JB, Ortiz JV, Cui Q, Baboul AG, Clifford S, Cioslowski J, Stefanov BB, Liu G, LiashenkoA, Piskorz P, Komaromi I, Martin RL, Fox DJ, Keith T, Al-Laham MA, Peng CY, Nanayakkara A, Challacombe M, Gill PMW, Johnson B, Chen W, Wong MW, Gonzalez C, Pople JA (2003) Gaussian 03, revision B.03. Gaussian, Pittsburgh, PA